



# Geophysical Research Letters

## RESEARCH LETTER

10.1002/2017GL076382

### Key Points:

- A sudden decrease in the solar wind dynamic pressure caused the prompt disappearance of magnetosonic waves
- A sudden increase in the solar wind dynamic pressure caused the prompt emergence of magnetosonic waves
- The adiabatic deceleration or acceleration of the ring current protons explained the evolution of magnetosonic waves

### Supporting Information:

- Supporting Information S1

### Correspondence to:

Z. Su,  
szpe@mail.ustc.edu.cn

### Citation:

Liu, N., Su, Z., Zheng, H., Wang, Y., & Wang, S. (2018). Prompt disappearance and emergence of radiation belt magnetosonic waves induced by solar wind dynamic pressure variations. *Geophysical Research Letters*, 45, 585–594.  
<https://doi.org/10.1002/2017GL076382>

Received 12 NOV 2017

Accepted 16 JAN 2018

Accepted article online 22 JAN 2018

Published online 30 JAN 2018

## Prompt Disappearance and Emergence of Radiation Belt Magnetosonic Waves Induced by Solar Wind Dynamic Pressure Variations

Nigang Liu<sup>1,2,3</sup> , Zhenpeng Su<sup>1,2</sup> , Huinan Zheng<sup>1,2</sup> , Yuming Wang<sup>1</sup> , and Shui Wang<sup>1</sup>

<sup>1</sup>CAS Key Laboratory of Geospace Environment, Department of Geophysics and Planetary Sciences, University of Science and Technology of China, Hefei, China, <sup>2</sup>Collaborative Innovation Center of Astronautical Science and Technology, University of Science and Technology of China, Hefei, China, <sup>3</sup>Mengcheng National Geophysical Observatory, School of Earth and Space Sciences, University of Science and Technology of China, Hefei, China

**Abstract** Magnetosonic waves are highly oblique whistler mode emissions transferring energy from the ring current protons to the radiation belt electrons in the inner magnetosphere. Here we present the first report of prompt disappearance and emergence of magnetosonic waves induced by the solar wind dynamic pressure variations. The solar wind dynamic pressure reduction caused the magnetosphere expansion, adiabatically decelerated the ring current protons for the Bernstein mode instability, and produced the prompt disappearance of magnetosonic waves. On the contrary, because of the adiabatic acceleration of the ring current protons by the solar wind dynamic pressure enhancement, magnetosonic waves emerged suddenly. In the absence of impulsive injections of hot protons, magnetosonic waves were observable even only during the time period with the enhanced solar wind dynamic pressure. Our results demonstrate that the solar wind dynamic pressure is an essential parameter for modeling of magnetosonic waves and their effect on the radiation belt electrons.

## 1. Introduction

The Earth's outer radiation belt electrons are highly dynamical in response to solar wind structures and magnetospheric activities (Baker et al., 1998; Li, 2001; Reeves et al., 2003, 2013; Su et al., 2014; Su, Zhu, Xiao, Zong, et al., 2015; Thorne et al., 2013) and pose a significant radiation hazard for both spacecraft and astronauts in the geospace environment (Baker et al., 1994; Wrenn, 1995). Hence, understanding the physical processes of electron acceleration, loss, and transport is of great interest to the radiation belt community. Specifically, the magnetosonic waves have been proposed to contribute to the electron acceleration via Landau resonance (Horne et al., 2007), bounce resonance (Roberts & Schulz, 1968; Shprits, 2009), or transit time scattering (Bortnik & Thorne, 2010). An observable signature of magnetosonic wave acceleration is the formation of butterfly pitch angle distributions of energetic electrons, as illustrated in the recent event (Li, 2016; Xiao et al., 2015) and statistical (Yang et al., 2017) studies.

Accurate information on the global spatiotemporal distribution of magnetosonic waves is important to understand and predict the evolution of radiation belt electrons. The Bernstein mode instability associated with proton ring distributions can generate the magnetosonic emissions at frequencies close to the local proton gyrofrequency harmonics (Balikhin et al., 2015; Boardsen et al., 1992; Curtis & Wu, 1979; Gary et al., 2010; Gulelmi et al., 1975; Horne et al., 2000; Meredith et al., 2008; Perraut et al., 1982). These whistler mode emissions with quasi-perpendicular wave vectors occur primarily within a few degrees latitude of the magnetic equatorial plane (Gurnett, 1976; Némec et al., 2005; Russell et al., 1970; Santolík, Pickett, Gurnett, Maksimovic, et al., 2002; Tsurutani et al., 2014) but propagate broadly in the radial and azimuthal directions (Chen & Thorne, 2012; Horne & Miyoshi, 2016; Horne et al., 2000; Kasahara et al., 1994; Ma et al., 2014; Némec et al., 2013; Santolík et al., 2016; Su et al., 2017). Extensive statistical studies have shown the geomagnetic activity dependence of magnetosonic waves (Boardsen et al., 2016; Hrbáčková et al., 2015; Ma et al., 2013; Meredith et al., 2008; Némec et al., 2015; Shprits et al., 2013), and recent studies (Kim & Chen, 2016; Kim & Shprits, 2017) have introduced the importance of solar wind parameters in the modeling of magnetosonic waves. The changes of solar wind conditions and geomagnetic indices are thought to take a time delay of several hours to substantially affect the

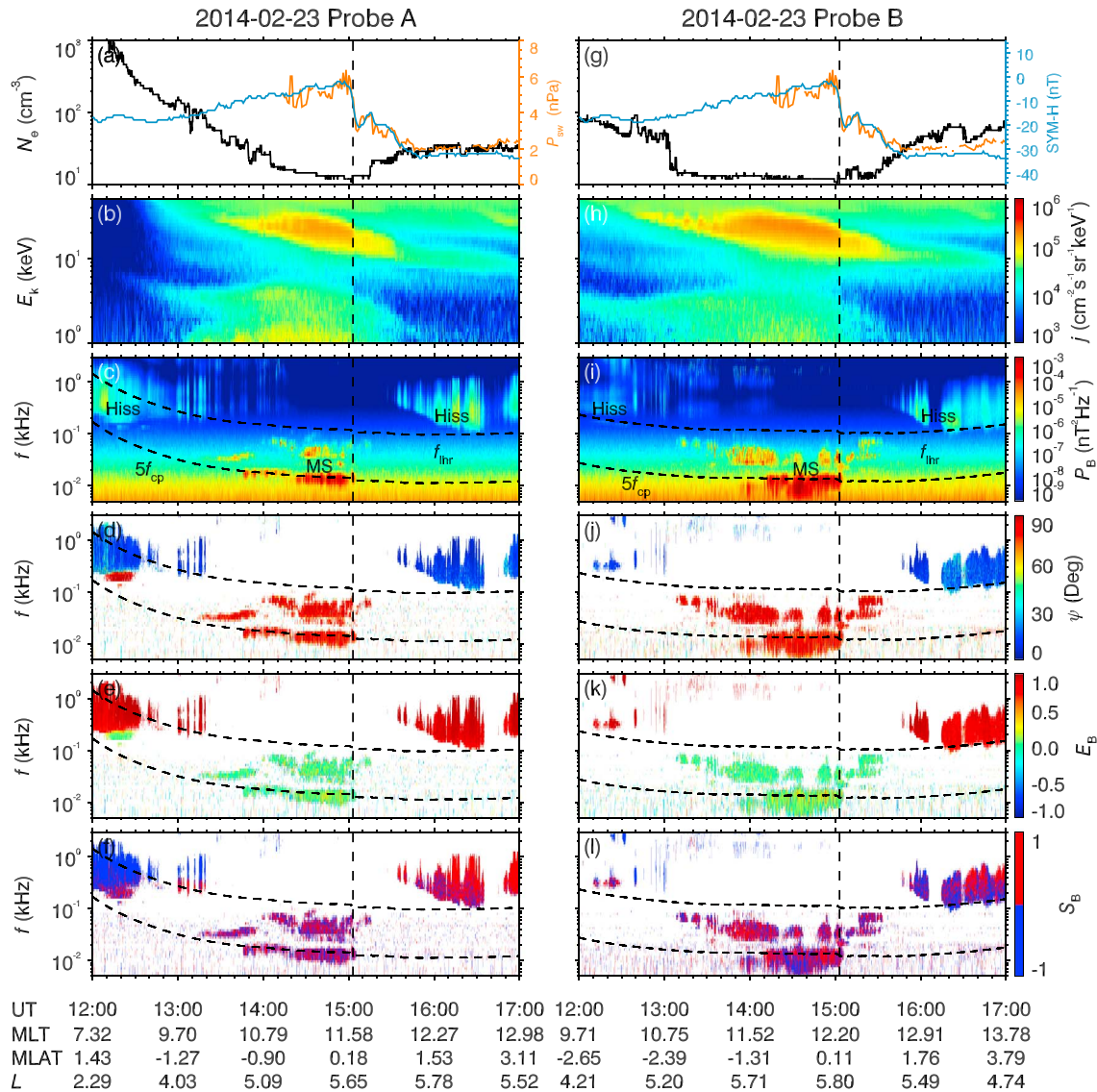


**Figure 1.** Overview of the magnetosonic wave event on 23 February 2014: (a, g) geomagnetic activity index  $SYM-H$ , background electron density  $N_e$ , and solar wind dynamic pressure  $P_{sw}$ ; (b, h) spin-averaged proton flux  $j$ ; (c, i) wave power spectral density  $P_B$ ; (d, j) wave normal angle  $\psi$ ; (e, k) wave ellipticity  $E_B$  (negative for left-hand polarization and positive for right-handed polarization); (f, l) sign of field-aligned component of Poynting flux  $S_B$  (positive for parallel orientation and negative for antiparallel orientation). The vertical dashed lines mark the arrival of the solar wind dynamic pressure pulse, and the other dashed lines represent the lower hybrid frequency  $f_{lhr}$  and fifth harmonic of equatorial proton gyrofrequency  $f_{cp}$ .

global distributions of magnetosonic waves in the previous modeling works (Kim & Chen, 2016; Kim & Shprits, 2017). Such a time delay may be interpreted as the timescale for solar wind-magnetosphere coupling and hot particle transport. However, the solar wind disturbances can pass through the dayside magnetosphere on a timescale of several minutes, and their immediate impacts on the magnetosonic waves remain unclear.

In this letter, we present several representative events of magnetosonic waves observed by the Van Allen Probes mission (Mauk et al., 2013) during the periods with sudden changes in the solar wind dynamic pressure. Our results demonstrate that the solar wind dynamic pressure variations can cause the prompt disappearance or emergence of magnetosonic waves by adiabatically changing the ring current proton distributions.

## 2. Data and Method

The Van Allen Probes mission contains two spacecraft in the highly elliptical orbits with the perigees  $\sim 0.1 R_E$  and the apogees  $\sim 6 R_E$ . In this study, we mainly use the data obtained by the Electric Field and Wave (EFW)

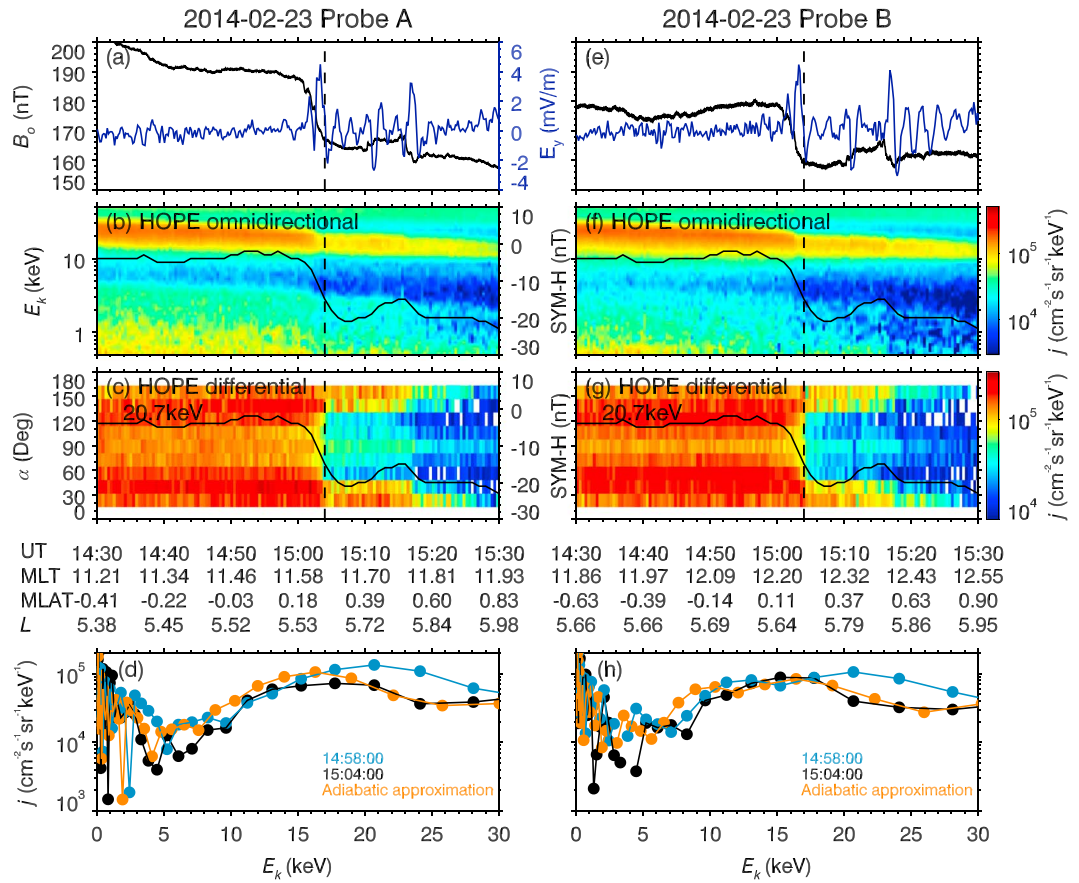


**Figure 2.** Electromagnetic fields and hot proton distributions around the pulse time on 23 February 2014: (a, e) magnetic field magnitude  $B_o$  and y component electric field  $E_y$  in the mGSE coordinate system, (b, c, f, and g) color-coded proton omnidirectional/differential flux  $j$ , and (d, h) observation and adiabatic approximation of the proton flux  $j$  at 90° pitch angle. In Figures 2b, 2c, 2f, and 2g, the black lines represent the SYM-H indices. The vertical dashed lines mark the arrival of the solar wind dynamic pressure pulse.

instrument (Wygant et al., 2013), the Electric and Magnetic Field Instrument and Integrated Science (EMFISIS) suite (Kletzing et al., 2013), and the Energetic Particle, Composition and Thermal Plasma Suite (ECT) (Spence et al., 2013).

The EFW instrument measured the local electric field  $\mathbf{E}$  in the modified geocentric solar ecliptic (mGSE) coordinate system (Wygant et al., 2013). The triaxial fluxgate magnetometer (MAG) of the EMFISIS suite detected the local magnetic field  $\mathbf{B}_o$ , and we estimate the corresponding equatorial magnetic field as  $B_e = B_o B_{Me} / B_{Mo}$  with the ratio  $B_{Me} / B_{Mo}$  between equatorial and local magnetic fields in the TS04 model (Tsyganenko & Sitnov, 2005). The Waveform Receiver (WFR) of the EMFISIS Waves instrument provided the wave spectral matrix from 5 Hz to 10 kHz. The frequency resolution of the onboard spectra of WFR is too low to display the discrete structures of magnetosonic waves, and we perform the fast Fourier transform (FFT) on the local magnetic fields to obtain the high-resolution wave spectral matrix below 32 Hz. On the basis of these spectral matrices, we can calculate the Poynting vector (Santolík et al., 2010), the wave vector direction, and the planarity and ellipticity of wave polarization (Santolík, Pickett, Gurnett, & Storey, 2002; Santolík et al., 2003). Following the previous study (Kurth et al., 2014), we infer the cold electron density  $N_e$  from the measurement of the upper hybrid resonance band by the High-Frequency Receiver (HFR) of the EMFISIS Waves instrument. In the low-density region ( $N_e < 10 \text{ cm}^{-3}$ ) with the upper hybrid resonance frequency below the lower-frequency limit of HFR, we estimate the density from the previous empirical model (Sheeley et al., 2001). The Helium Oxygen Proton Electron (HOPE) (Funsten et al., 2013) and the Magnetic Electron Ion Spectrometer (MagEIS) (Blake et al., 2013) of the ECT suite gave the flux  $j$  of hot (0.1–300 keV) protons.

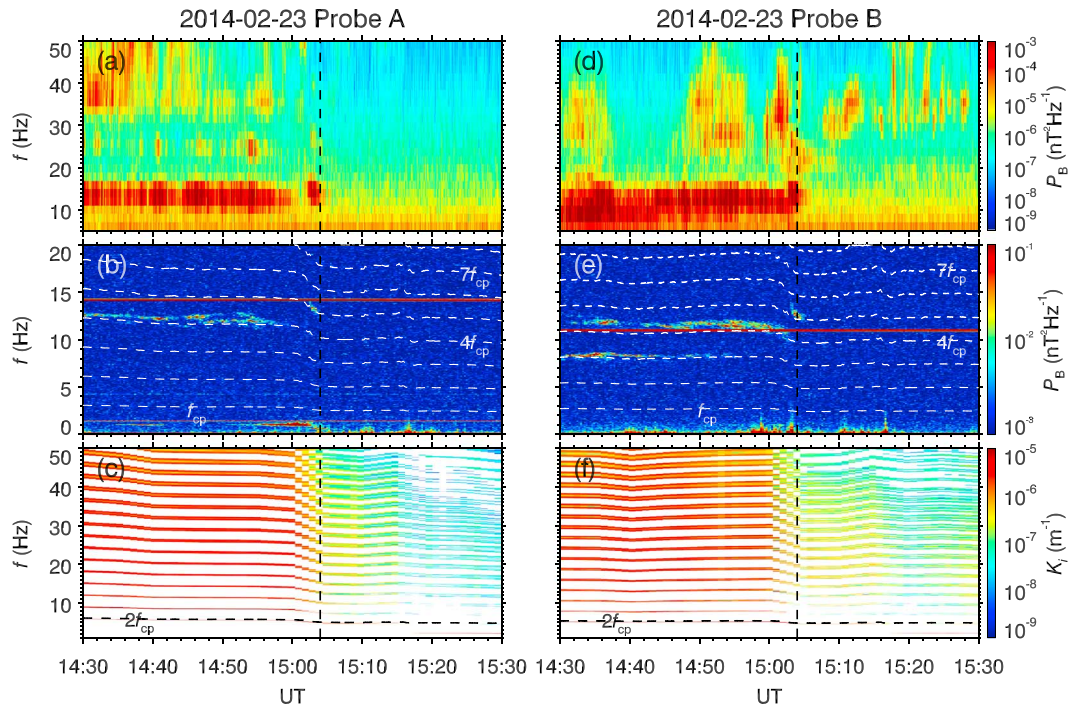


**Figure 3.** Bernstein mode instability for magnetosonic waves around the pulse time on 23 February 2014: wave power  $P_B$  observed by (a, d) WFR and (b, e) MAG-FFT; (c, f) convective growth rate  $K_i$ . In Figures 3b, 3c, 3e, and 3f, the dashed lines represent the proton gyrofrequency harmonics. The vertical dashed lines mark the arrival of the solar wind dynamic pressure pulse.

Following the approach of Kennel (1966), we can obtain the temporal growth rate

$$\gamma = -\frac{D_i}{\partial D^0 / \partial \omega}, \quad (1)$$

and the convective growth rate

$$K_i = \gamma / |\mathbf{V}_g| \quad (2)$$

for a plasma wave with the angular frequency  $\omega$ , the wave vector  $\mathbf{k} = k \cos \psi \mathbf{e}_{\parallel} + k \sin \psi \mathbf{e}_{\perp}$ , and the wave normal angle  $\psi$ . Here  $D^0$  and  $D_i$  are the real and imaginary parts of the dispersion relation  $D(\omega, k, \psi) = D^0 + iD_i$  listed in the previous work (Chen et al., 2010, equation (A3)). In the present study of magnetosonic waves, the expression of  $D_i$  depends on the hot proton phase space density  $F = j/p^2$  and its derivatives with respect to energy and pitch angle (Chen et al., 2010, equation (A4)). To reduce the noise, we compute a smooth cubic spline approximation (Reinsch, 1967) to the proton pitch angle distribution at each energy channel (see more details in Text S1 of the supporting information) and then evaluate those required derivatives using the B-spline interpolation (De Boor, 1977) in the pitch angle-energy space.

### 3. Disappearance of Magnetosonic Waves by Solar Wind Dynamic Pressure Decrease

Figure 1 gives an overview of the magnetosonic wave event associated with a sudden decrease of the solar wind dynamic pressure on 23 February 2014. During the time period of interest, the Van Allen Probes were located near the equator ( $|MLAT| < 4^\circ$ ) in the dayside sector ( $7 < |MLT| < 14$ ). Initially, both probes were in the high-density ( $N_e > 100 \text{ cm}^{-3}$ ) plasmasphere and observed the plasmaspheric hiss. At 13:07 UT, Probe B passed through the plasmapause characterized as a sudden decrease in density, and about 30 min later, Probe A went outside the high-density plasmasphere. In the low-density region, both probes received the magnetosonic wave signals (with the linear polarization  $E_B \approx 0$ , the quasi-perpendicular normal angle  $\psi > 80^\circ$ , and the bidirectional Poynting vector) below the lower hybrid frequency. The temporal evolution of magnetosonic waves tended to follow the variation of the lower hybrid frequency and the proton gyrofrequency harmonics, indicating that these waves were likely generated by the local ring distributions of hot

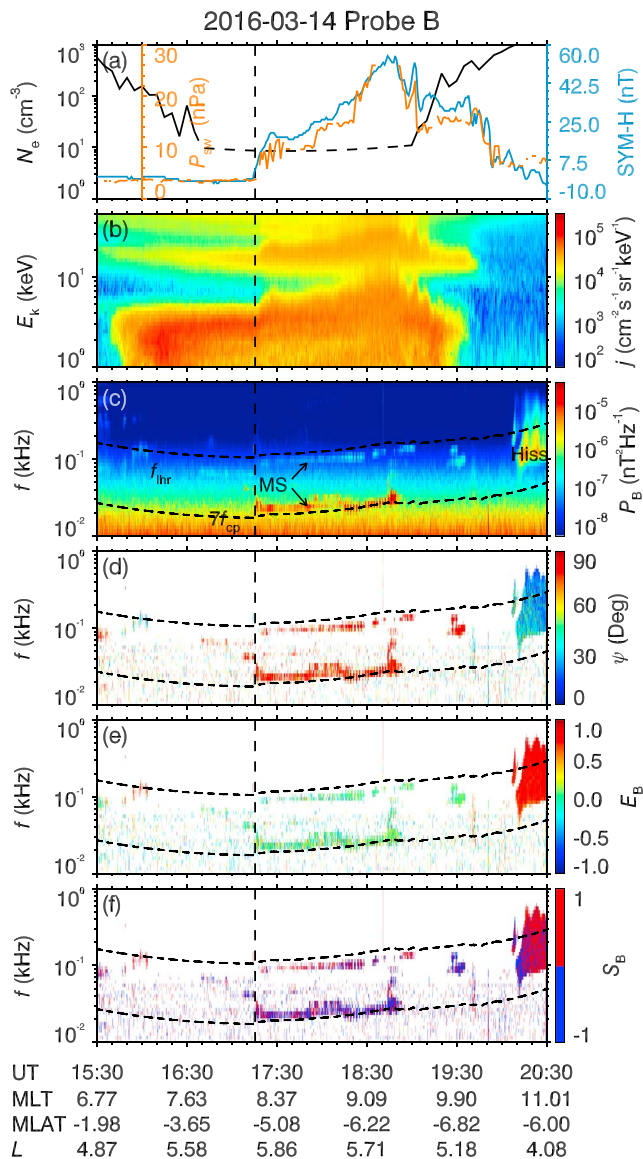


**Figure 4.** Overview of the magnetosonic wave event on 14 March 2016, with the same format as in Figure 1.

waves is allowed above 4 Hz (from second to seventeenth proton gyrofrequency harmonics), consistent with the observations of both WFR and MAG-FFT. The peak growth rates of magnetosonic waves with the normal angle  $\psi = 89.5^\circ$  are about  $K_i \sim 10^{-5} \text{ m}^{-1}$ , comparable to the previous numerical calculations (Chen et al., 2010). After the pulse, the modeled growth rates decrease by approximately 10 times, responsible for the sudden disappearance of intense magnetosonic waves below 20 Hz. During the period of 15:10–15:30 UT, the modeled growth rates of Probe B are larger than those of Probe A, qualitatively explaining the residual occurrence of some weak sporadic magnetosonic waves above 20 Hz for Probe B.

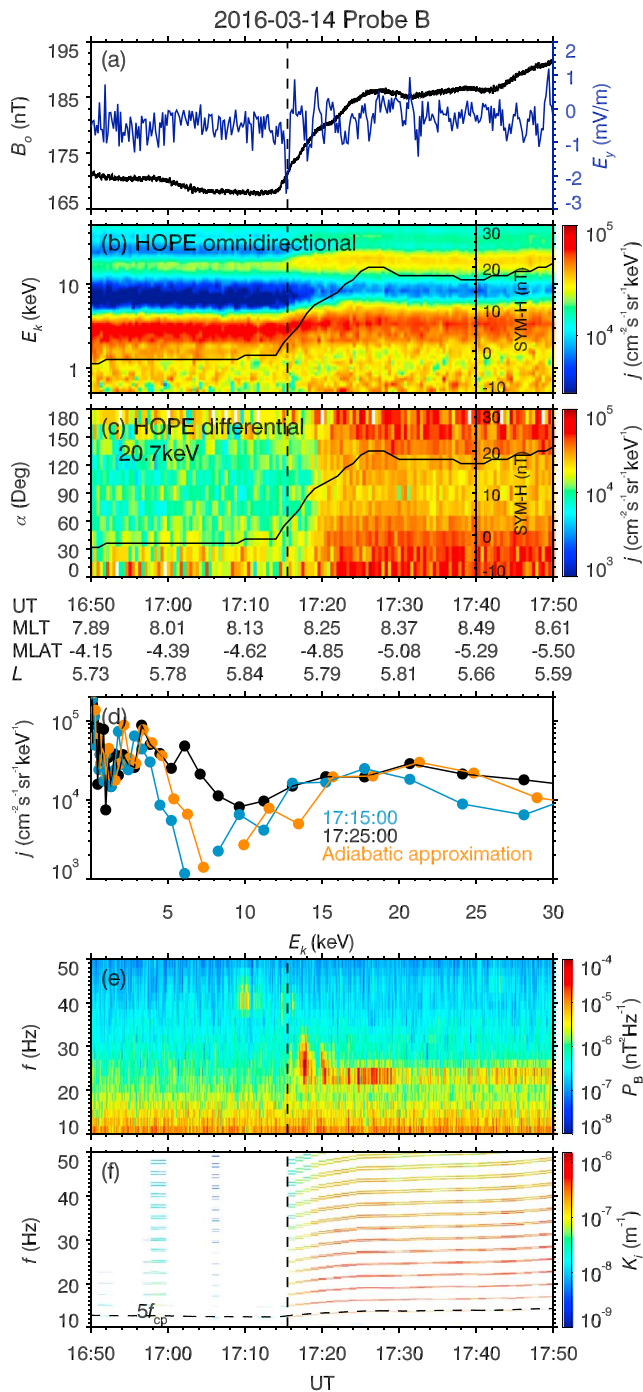
#### 4. Emergence of Magnetosonic Waves by Solar Wind Dynamic Pressure Increase

Figure 4 shows an overview of the magnetosonic wave event associated with an interplanetary shock on 14 March 2016. In this event, Probe A was near the perigee and unable to observe the shock influence on magnetosonic waves. Before the shock, magnetosonic waves were nearly unobservable for Probe B both inside and outside the plasmasphere. At 17:15:30 UT, the interplanetary shock hit the magnetosphere, causing the increase of SYM-H index from -3 to 20 nT. In response to the shock compression, the hot proton fluxes exhibited a significant enhancement over a wide energy range, and the magnetosonic waves close to the lower

protons around 20 keV. At 15:03 UT, the solar wind dynamic pressure suddenly decreased from 6 nPa to 3 nPa. Correspondingly, the SYM-H index decreased from 0 to -20 nT, implying an expansion of the global magnetosphere. In response to this solar wind dynamic pressure pulse, the proton fluxes above 10 keV decreased obviously and the most intense magnetosonic waves below 20 Hz disappeared abruptly. In the subsequent time period of > 2 h, the magnetosphere remained in an expanded state ( $\text{SYM-H} \approx -30 \text{ nT}$ ) and both probes did not observe the recovery of intense magnetosonic waves.

Figure 2 plots the electromagnetic fields and the hot proton distributions around the solar wind dynamic pressure pulse. Roughly speaking, two probes observed the consistent responses of electromagnetic fields and hot protons to the pressure pulse. After the pulse, the local magnetic fields decreased by  $\sim 25 \text{ nT}$ , comparable to the variation of SYM-H calculated from the ground-based magnetic stations. The local electric fields appeared to be wave like with a peak amplitude of  $\sim 4 \text{ mV/m}$ , probably induced by the changing magnetic field. Given the temporal profiles of the local magnetic field, we adiabatically transform the  $90^\circ$  proton phase space density from the prepulse time (14:58 UT) to the postpulse time (15:04 UT). One can find that the adiabatic approximation can well explain the hot proton flux variation in this event. The adiabatic decrease of proton fluxes become most significant around 20 keV because the prepulse phase space density  $\sim 20 \text{ keV}$  had a steep negative gradient with respect to energy. The adiabatic energy change usually increases with the pitch angle approaching  $90^\circ$  (see simulations by Kim et al., 2010; Su et al., 2010a, 2011), yielding the most significant reduction of proton fluxes at the  $90^\circ$  pitch angle.

Figure 3 compares the observed magnetosonic wave spectra to the linear convective growth rates. The magnetosonic wave spectra observed by the WFR can be divided into two parts: continuous intense signals below 20 Hz and intermittent weak signals above 20 Hz. The intense signals of the WFR corresponded to the fourth and third magnetosonic emission lines observed by the MAG-FFT, while the weak signals of the WFR were below the detection threshold level of the MAG-FFT. In Figure S1 of the supporting information, we present several examples of modeled and observed proton phase space distributions, and the modeled distributions appear to be in a reasonable agreement with the observations both before and after the solar wind dynamic pressure pulse. The temporal variation of the obtained wave convective growth rate is able to qualitatively explain the evolution of magnetosonic waves in this event. Before the pulse, the modeled growth



**Figure 5.** Electromagnetic fields, hot proton distributions, and wave instabilities around the pulse time on 14 March 2016: (a) magnetic field magnitude  $B_o$  and electric field  $E_y$ , (b, c) color-coded proton omnidirectional/differential flux  $j$ , (d) observation and adiabatic approximation of the proton flux  $j$  at 90° pitch angle, (e) WRF wave power  $P_B$ , and (f) convective growth rate  $K_i$ . The vertical dashed lines mark the arrival of the solar wind dynamic pressure pulse.

promoted the excitation of magnetosonic waves. The physical processes acting in the two events could be roughly considered the inverse of each other. These phenomena are essentially different from the observations in a recent study of “amplification and attenuation of magnetosonic waves associated with the

hybrid frequency and the seventh proton gyrofrequency harmonic emerged suddenly. In the subsequent period of 2 h, the hot proton fluxes were further enhanced as the solar wind dynamic pressure increased continuously. After 19:05 UT, Probe B went away from the equatorial region and can no longer detect the magnetosonic waves.

As demonstrated in Figure 5, the evolution of fields, particles, and waves can be interpreted as an “inverse” process of that in the 23 February 2014 event. The shock compression produced the increase of the local magnetic field by 20 nT, the wave-like electric fields with a peak amplitude of 2 mV/m, and the enhancement of the hot proton fluxes by up to 3 times. Similar to the previous event, the proton fluxes exhibited the most significant variations at 90° pitch angle above 10 keV. The adiabatic approximation can well explain the observed proton flux enhancement above 10 keV, while the data gap of the preshock proton flux from 6 keV to 8 keV does not allow a reasonable reproduction of the postshock 7–10 keV proton fluxes. In this event, the magnetosonic waves were not well recorded by the MAG-FFT probably because the wave intensity was below the threshold of MAG-FFT. We compare the WFR spectra to the calculated convective growth rates of magnetosonic waves at the normal angle  $\psi=89.5^\circ$  (with the modeled proton distributions in Figure S2 of the supporting information). Before the shock, the magnetosonic waves are found to have quite weak growth rates ( $K_i < 10^{-9} \text{ m}^{-1}$ ) or experience a strong damping ( $K_i < 0$ ). After the shock, the modeled growth rates reach up to about  $K_i \sim 10^{-6} \text{ m}^{-1}$  and peak around the sixth to tenth proton gyrofrequency harmonics, qualitatively explaining the emergence of magnetosonic waves below 30 Hz.

## 5. Conclusions and Discussions

Magnetosonic waves are able to transfer energy from the ring current protons to the radiation belt electrons in the inner magnetosphere (e.g., Bortnik & Thorne, 2010; Chen et al., 2015; Horne et al., 2007; Li, 2016; Shprits, 2009; Xiao et al., 2015; Yang et al., 2017). Understanding and forecasting the radiation belt environment need the accurate knowledge of the spatiotemporal distribution of magnetosonic waves (e.g., Fok et al., 2008; Glauert et al., 2014; Shprits et al., 2009; Su et al., 2010b, 2011; Subbotin et al., 2010; Tu et al., 2013; Varotsou et al., 2005, 2008). In contrast to the numerous studies of the correlations between geomagnetic activities and magnetosonic waves (e.g., Boardsen et al., 2016; Hrbáčková et al., 2015; Ma et al., 2013; Meredith et al., 2008; Némec et al., 2015; Shprits et al., 2013), there have been relatively few works to evaluate the direct influences of solar wind variations on magnetosonic waves (Kim & Chen, 2016; Kim & Shprits, 2017). In these limited studies, the changes of solar wind parameters were thought to affect the global distribution of magnetosonic wave with a time delay of several hours (Kim & Chen, 2016; Kim & Shprits, 2017). Here we present the first report of prompt disappearance and emergence of magnetosonic waves induced by the solar wind dynamic pressure variations. On 23 February 2014, the sudden decrease in the solar wind dynamic pressure caused the expansion of the magnetosphere and the decrease of the local magnetic field. The adiabatically decelerated ring current protons became unfavorable for the Bernstein mode instability, producing no observable magnetosonic waves. On 14 March 2016, the interplanetary shock compressed the magnetosphere, accelerated the ring current protons approximately in an adiabatic way, and

compression and expansion of the Earth's magnetosphere" (Li, 2017). In their study (Li, 2017), there were step-like variations in the background plasma density but gradual variations in the solar wind dynamic pressure for the amplification and attenuation of magnetosonic waves. As a result, it was difficult to differentiate between the contributions of the solar wind dynamic pressure variation and the local plasma density modulation (Chen & Thorne, 2012; Ma et al., 2014; Yuan et al., 2017) to the evolution of magnetosonic waves. In contrast, our present data and modeling, without any observable plasma density modulations, directly link the magnetosonic wave evolution to the solar wind dynamic pressure sudden variations.

In fact, these phenomena reported here are not rare in the Van Allen Probes data. Figure S3 of the supporting information presents another magnetosonic wave event associated with the solar wind dynamic pressure variations on 4 August 2017. In the time period of interest, there was no impulsive injection of hot protons, and the solar wind dynamic pressure essentially controlled the spatiotemporal distribution of magnetosonic waves. At 03:33 UT, the increase in the solar wind dynamic pressure caused the emergence of magnetosonic waves; at 05:24 UT, the decrease in the solar wind dynamic pressure yielded the disappearance of magnetosonic waves. The intense magnetosonic waves were observable only in the period from 03:33 UT to 05:24 UT with the enhanced solar wind dynamic pressure. Other interesting features of Figure S3 are the dramatic responses of whistler mode hiss and chorus waves to the solar wind dynamic pressure variations, which have been studied recently in detail (Liu, Su, Gao, Zheng, et al., 2017; Liu, Su, Gao, Reeves, et al., 2017; Su, Zhu, Xiao, Zheng, et al., 2015; Yue et al., 2017). For the electromagnetic ion cyclotron waves destabilized by the comparable energy protons to those for the magnetosonic wave excitation, the solar wind compression has long been recognized as an important trigger (e.g., Anderson & Hamilton, 1993; Cho et al., 2017; McCollough et al., 2010; Usanova et al., 2008). The solar wind dynamic pressure fluctuations can also directly drive the Pc4–Pc5 ultralow-frequency waves in the dayside magnetosphere, as shown in previous numerical (e.g., Claudepierre et al., 2009) and observational (e.g., Liu, 2010; Rae et al., 2012; Su, Zhu, Xiao, Zong, et al., 2015; Zhang et al., 2010) studies. All these waves have been frequently invoked to explain the acceleration, transport, and loss of the radiation belt electrons (Thorne, 2010). Our present findings, together with the early studies mentioned above, highlight the importance of the solar wind dynamic pressure in the spatiotemporal distribution of these magnetospheric waves and in the wave-driven evolution of the radiation belt electrons.

#### Acknowledgments

We acknowledge EMFISIS, ECT, and EFW teams for the use of Van Allen Probes data. Data are available from the following websites: <http://emfisis.physics.uiowa.edu/Flight/>, [http://www.rbsp-ect.lanl.gov/data\\_pub/](http://www.rbsp-ect.lanl.gov/data_pub/), and <http://www.space.umn.edu/rbspefw-data/>. This work was supported by the National Natural Science Foundation of China grants 41774170, 41631071, 41422405, 41274174, 41174125, 41131065, 41421063, 41231066, and 41304134; the Chinese Academy of Sciences grants KZCX2-EW-QN510 and KZZD-EW-01-4; the CAS Key Research Program of Frontier Sciences grant QYZDB-SSW-DQC015; the National Key Basic Research Special Foundation of China grant 2011CB811403; and the Fundamental Research Funds for the Central Universities WK2080000077.

#### References

- Anderson, B. J., & Hamilton, D. C. (1993). Electromagnetic ion cyclotron waves stimulated by modest magnetospheric compressions. *Journal of Geophysical Research*, 98, 11,369–11,382. <https://doi.org/10.1029/93JA00605>
- Baker, D. N., Kanekal, S., Blake, J. B., Klecker, B., & Rostoker, G. (1994). Satellite anomalies linked to electron increase in the magnetosphere. *EOS Transactions*, 75, 401–405. <https://doi.org/10.1029/94EO01038>
- Baker, D. N., Pulkkinen, T. I., Li, X., Kanekal, S. G., Blake, J. B., Selesnick, R. S., ... Rostoker, G. (1998). Coronal mass ejections, magnetic clouds, and relativistic magnetospheric electron events: ISTP. *Journal of Geophysical Research*, 103, 17,279–17,292. <https://doi.org/10.1029/97JA03329>
- Balikhin, M. A., Shprits, Y. Y., Walker, S. N., Chen, L., Cornilleau-Wehrlin, N., Dandouras, I., ... Weiss, B. (2015). Observations of discrete harmonics emerging from equatorial noise. *Nature Communications*, 6, 7703. <https://doi.org/10.1038/ncomms8703>
- Blake, J. B., Carranza, P. A., Claudepierre, S. G., Clemons, J. H., Crain, W. R., Dotan, Y., ... Zakrzewski, M. P. (2013). The Magnetic Electron Ion Spectrometer (MagEIS) instruments aboard the Radiation Belt Storm Probes (RBSP) spacecraft. *Space Science Reviews*, 179, 383–421. <https://doi.org/10.1007/s11214-013-9991-8>
- Boardsen, S. A., Gallagher, D. L., Gurnett, D. A., Peterson, W. K., & Green, J. L. (1992). Funnel-shaped, low-frequency equatorial waves. *Journal of Geophysical Research*, 97(14), 14,967–14,976. <https://doi.org/10.1029/92JA00827>
- Boardsen, S. A., Hospodarsky, G. B., Kletzing, C. A., Engebretson, M. J., Pfaff, R. F., Wygant, J. R., ... De Pascuale, S. (2016). Survey of the frequency dependent latitudinal distribution of the fast magnetosonic wave mode from Van Allen Probes Electric and Magnetic Field Instrument and Integrated Science waveform receiver plasma wave analysis. *Journal of Geophysical Research: Space Physics*, 121, 2902–2921. <https://doi.org/10.1002/2015JA021844>
- Bortnik, J., & Thorne, R. M. (2010). Transit time scattering of energetic electrons due to equatorially confined magnetosonic waves. *Journal of Geophysical Research*, 115, A07213. <https://doi.org/10.1029/2010JA015283>
- Chen, L., & Thorne, R. M. (2012). Perpendicular propagation of magnetosonic waves. *Geophysical Research Letters*, 39, L14102. <https://doi.org/10.1029/2012GL052485>
- Chen, L., Maldonado, A., Bortnik, J., Thorne, R. M., Li, J., Dai, L., & Zhan, X. (2015). Nonlinear bounce resonances between magnetosonic waves and equatorially mirroring electrons. *Journal of Geophysical Research: Space Physics*, 120, 6514–6527. <https://doi.org/10.1002/2015JA021174>
- Chen, L., Thorne, R. M., Jordanova, V. K., & Horne, R. B. (2010). Global simulation of magnetosonic wave instability in the storm time magnetosphere. *Journal of Geophysical Research*, 115, A11222. <https://doi.org/10.1029/2010JA015707>
- Cho, J.-H., Lee, D.-Y., Noh, S.-J., Kim, H., Choi, C. R., Lee, J., & Hwang, J. (2017). Spatial dependence of electromagnetic ion cyclotron waves triggered by solar wind dynamic pressure enhancements. *Journal of Geophysical Research: Space Physics*, 122, 5502–5518. <https://doi.org/10.1002/2016JA023827>
- Claudepierre, S. G., Wiltberger, M., Elkington, S. R., Lotko, W., & Hudson, M. K. (2009). Magnetospheric cavity modes driven by solar wind dynamic pressure fluctuations. *Geophysical Research Letters*, 36, L13101. <https://doi.org/10.1029/2009GL039045>
- Curtis, S. A., & Wu, C. S. (1979). Gyroharmonic emissions induced by energetic ions in the equatorial plasmasphere. *Journal of Geophysical Research*, 84, 2597–2607. <https://doi.org/10.1029/JA084iA06p02597>

- De Boor, C. (1977). Package for calculating with B-splines. *SIAM Journal on Numerical Analysis*, 14(3), 441–472.
- Fok, M.-C., Horne, R. B., Meredith, N. P., & Glauert, S. A. (2008). Radiation Belt Environment model: Application to space weather nowcasting. *Journal of Geophysical Research*, 113, A03S08. <https://doi.org/10.1029/2007JA012558>
- Funsten, H. O., Skoug, R. M., Guthrie, A. A., MacDonald, E. A., Baldonado, J. R., Harper, R. W., ... Chen, J. (2013). Helium, Oxygen, Proton, and Electron (HOPE) mass spectrometer for the Radiation Belt Storm Probes mission. *Space Science Reviews*, 179, 423–484. <https://doi.org/10.1007/s11214-013-9967>
- Gary, S. P., Liu, K., Winske, D., & Denton, R. E. (2010). Ion Bernstein instability in the terrestrial magnetosphere: Linear dispersion theory. *Journal of Geophysical Research*, 115, A12209. <https://doi.org/10.1029/2010JA015965>
- Glauert, S. A., Horne, R. B., & Meredith, N. P. (2014). Three-dimensional electron radiation belt simulations using the BAS Radiation Belt Model with new diffusion models for chorus, plasmaspheric hiss, and lightning-generated whistlers. *Journal of Geophysical Research: Space Physics*, 119, 268–289. <https://doi.org/10.1002/2013JA019281>
- Gulelmi, A. V., Klaine, B. I., & Potapov, A. S. (1975). Excitation of magnetosonic waves with discrete spectrum in the equatorial vicinity of the plasmapause. *Planetary and Space Science*, 23, 279–286. [https://doi.org/10.1016/0032-0633\(75\)90133-6](https://doi.org/10.1016/0032-0633(75)90133-6)
- Gurnett, D. A. (1976). Plasma wave interactions with energetic ions near the magnetic equator. *Journal of Geophysical Research*, 81, 2765–2770. <https://doi.org/10.1029/JA081i016p02765>
- Horne, R. B., & Miyoshi, Y. (2016). Propagation and linear mode conversion of magnetosonic and electromagnetic ion cyclotron waves in the radiation belts. *Geophysical Research Letters*, 43, 10,034–10,039. <https://doi.org/10.1002/2016GL070216>
- Horne, R. B., Thorne, R. M., Glauert, S. A., Meredith, N. P., Pokhotelov, D., & Santolík, O. (2007). Electron acceleration in the Van Allen radiation belts by fast magnetosonic waves. *Geophysical Research Letters*, 34, L17107. <https://doi.org/10.1029/2007GL030267>
- Horne, R. B., Wheeler, G. V., & Alleyne, H. S. C. (2000). Proton and electron heating by radially propagating fast magnetosonic waves. *Journal of Geophysical Research*, 105, 27,597–27,610. <https://doi.org/10.1029/2000JA000018>
- Hrbáčková, Z., Santolík, O., Němec, F., Macúšová, E., & Cornilleau-Wehrlin, N. (2015). Systematic analysis of occurrence of equatorial noise emissions using 10 years of data from the Cluster mission. *Journal of Geophysical Research: Space Physics*, 120, 1007–1021. <https://doi.org/10.1002/2014JA020268>
- Kasahara, Y., Kenmochi, H., & Kimura, I. (1994). Propagation characteristics of the ELF emissions observed by the satellite Akebono in the magnetic equatorial region. *Radio Science*, 29, 751–767. <https://doi.org/10.1029/94RS00445>
- Kennel, C. (1966). Low-frequency whistler mode. *Physics of Fluids*, 9, 2190–2202. <https://doi.org/10.1063/1.1761588>
- Kim, K.-C., & Chen, L. (2016). Modeling the storm time behavior of the magnetosonic waves using solar wind parameters. *Journal of Geophysical Research: Space Physics*, 121, 446–458. <https://doi.org/10.1002/2015JA021716>
- Kim, K.-C., & Shprits, Y. (2017). Dependence of the amplitude of magnetosonic waves on the solar wind and AE index using Van Allen Probes. *Journal of Geophysical Research: Space Physics*, 122, 6022–6034. <https://doi.org/10.1002/2017JA024094>
- Kim, K. C., Lee, D., Kim, H., Lee, E. S., & Choi, C. R. (2010). Numerical estimates of drift loss and Dst effect for outer radiation belt relativistic electrons with arbitrary pitch angle. *Journal of Geophysical Research*, 115, A03208. <https://doi.org/10.1029/2009JA014523>
- Kletzing, C. A., Kurth, W. S., Acuna, M., MacDowall, R. J., Torbert, R. B., Averkamp, T., ... Tyler, J. (2013). The Electric and Magnetic Field Instrument Suite and Integrated Science (EMFISIS) on RBSP. *Space Science Reviews*, 179, 127–181. <https://doi.org/10.1007/s11214-013-9993-6>
- Kurth, W. S., Pascuale, S. D., Faden, J. B., Kletzing, C. A., Hospodarsky, G. B., Thaller, S., & Wygant, J. R. (2014). Electron densities inferred from plasma wave spectra obtained by the waves instrument on Van Allen Probes. *Journal of Geophysical Research: Space Physics*, 120, 904–914. <https://doi.org/10.1002/2014JA020857>
- Li, J., Ni, B., Ma, Q., Xie, L., Pu, Z., Fu, S., ... Summers, D. (2016). Formation of energetic electron butterfly distributions by magnetosonic waves via Landau resonance. *Geophysical Research Letters*, 43, 3009–3016. <https://doi.org/10.1002/2016GL067853>
- Li, L. Y., Liu, B., Yu, J., & Cao, J. B. (2017). The rapid responses of magnetosonic waves to the compression and expansion of Earth's magnetosphere. *Geophysical Research Letters*, 44, 11,239–11,247. <https://doi.org/10.1002/2017GL075649>
- Li, X., Baker, D. N., Kanekal, S. G.,Looper, M., & Temerin, M. (2001). Long term measurements of radiation belts by SAMPEX and their variations. *Geophysical Research Letters*, 28, 3827–3830. <https://doi.org/10.1029/2001GL013586>
- Liu, N., Su, Z., Gao, Z., Reeves, G. D., Zheng, H., Wang, Y., & Wang, S. (2017). Shock-induced disappearance and subsequent recovery of plasmaspheric hiss: Coordinated observations of RBSP, THEMIS, and POES satellites. *Journal of Geophysical Research: Space Physics*, 122, 10,421–10,435. <https://doi.org/10.1002/2017JA024470>
- Liu, N., Su, Z., Gao, Z., Zheng, H., Wang, Y., Wang, S., ... Wygant, J. R. (2017). Simultaneous disappearances of plasmaspheric hiss, exohiss, and chorus waves triggered by a sudden decrease in solar wind dynamic pressure. *Geophysical Research Letters*, 44, 52–61. <https://doi.org/10.1002/2016GL071987>
- Liu, W., Sarris, T. E., Li, X., Ergun, R., Angelopoulos, V., Bonnell, J., & Glassmeier, K. H. (2010). Solar wind influence on Pc4 and Pc5 ULF wave activity in the inner magnetosphere. *Journal of Geophysical Research*, 115, A12201. <https://doi.org/10.1029/2010JA015299>
- Ma, Q., Li, W., Chen, L., Thorne, R. M., Kletzing, C. A., Kurth, W. S., ... Spence, H. E. (2014). The trapping of equatorial magnetosonic waves in the Earth's outer plasmasphere. *Geophysical Research Letters*, 41, 6307–6313. <https://doi.org/10.1002/2014GL061414>
- Ma, Q., Li, W., Thorne, R. M., & Angelopoulos, V. (2013). Global distribution of equatorial magnetosonic waves observed by THEMIS. *Geophysical Research Letters*, 40, 1895–1901. <https://doi.org/10.1002/grl.50434>
- Mauk, B. H., Fox, N. J., Kanekal, S. G., Kessel, R. L., Sibeck, D. G., & Ukhorskiy, A. (2013). Science objectives and rationale for the Radiation Belt Storm Probes mission. *Space Science Reviews*, 179, 3–27. <https://doi.org/10.1007/s11214-012-9908-y>
- McCollough, J. P., Elkington, S. R., Usanova, M. E., Mann, I. R., Baker, D. N., & Kale, Z. C. (2010). Physical mechanisms of compressional EMIC wave growth. *Journal of Geophysical Research*, 115, A10214. <https://doi.org/10.1029/2010JA015393>
- Meredith, N. P., Horne, R. B., & Anderson, R. R. (2008). Survey of magnetosonic waves and proton ring distributions in the Earth's inner magnetosphere. *Journal of Geophysical Research*, 113, A06213. <https://doi.org/10.1029/2007JA012975>
- Němec, F., Santolík, O., Gerecová, K., Macúšová, E., de Conchy, Y., & Cornilleau-Wehrlin, N. (2005). Initial results of a survey of equatorial noise emissions observed by the Cluster spacecraft. *Planetary and Space Science*, 53, 291–298. <https://doi.org/10.1016/j.pss.2004.09.055>
- Němec, F., Santolík, O., Hrbáčková, Z., Pickett, J. S., & Cornilleau-Wehrlin, N. (2015). Equatorial noise emissions with quasiperiodic modulation of wave intensity. *Journal of Geophysical Research: Space Physics*, 120, 2649–2661. <https://doi.org/10.1002/2014JA020816>
- Němec, F., Santolík, O., Pickett, J. S., Hrbáčková, Z., & Cornilleau-Wehrlin, N. (2013). Azimuthal directions of equatorial noise propagation determined using 10 years of data from the Cluster spacecraft. *Journal of Geophysical Research: Space Physics*, 118, 7160–7169. <https://doi.org/10.1002/2013JA019373>
- Perraut, S., Roux, A., Robert, P., Gendrin, R., Sauvage, J.-A., Bosqued, J.-M., ... Korth, A. (1982). A systematic study of ULF waves above  $F_{H^+}$  from GEOS 1 and 2 measurements and their relationships with proton ring distributions. *Journal of Geophysical Research*, 87, 6219–6236. <https://doi.org/10.1029/JA087iA08p06219>

- Rae, I. J., Mann, I. R., Murphy, K. R., Ozeke, L. G., Milling, D. K., Chan, A. A., ... Honary, F. (2012). Ground-based magnetometer determination of in situ Pc4–5 ULF electric field wave spectra as a function of solar wind speed. *Journal of Geophysical Research*, 117, A04221. <https://doi.org/10.1029/2011JA017335>
- Reeves, G. D., McAdams, K. L., Friedel, R. H. W., & O'Brien, T. P. (2003). Acceleration and loss of relativistic electrons during geomagnetic storms. *Geophysical Research Letters*, 30(10), 1529. <https://doi.org/10.1029/2002GL016513>
- Reeves, G. D., Spence, H. E., Henderson, M. G., Morley, S. K., Friedel, R. H. W., Funsten, H. O., ... Niehof, J. T. (2013). Electron acceleration in the heart of the Van Allen radiation belts. *Science*, 341(6149), 991–994. <https://doi.org/10.1126/science.1237743>
- Reinsch, C. H. (1967). Smoothing by spline functions. *Numerische Mathematik*, 10(3), 177–183.
- Roberts, C. S., & Schulz, M. (1968). Bounce resonant scattering of particles trapped in the Earth's magnetic field. *Journal of Geophysical Research*, 73, 7361–7376. <https://doi.org/10.1029/JA073i023p07361>
- Russell, C. T., Holzer, R. E., & Smith, E. J. (1970). OGO 3 observations of ELF noise in the magnetosphere. 2. The nature of the equatorial noise. *Journal of Geophysical Research*, 75, 755–768. <https://doi.org/10.1029/JA075i004p00755>
- Santolík, O., Parrot, M., & Lefèuvre, F. (2003). Singular value decomposition methods for wave propagation analysis. *Radio Science*, 38(1), 1010. <https://doi.org/10.1029/2000RS002523>
- Santolík, O., Parrot, M., & Némec, F. (2016). Propagation of equatorial noise to low altitudes: Decoupling from the magnetosonic mode. *Geophysical Research Letters*, 43, 6694–6704. <https://doi.org/10.1002/2016GL069582>
- Santolík, O., Pickett, J. S., Gurnett, D. A., & Storey, L. R. O. (2002). Magnetic component of narrowband ion cyclotron waves in the auroral zone. *Journal of Geophysical Research*, 107(A12), 1444. <https://doi.org/10.1029/2001JA000146>
- Santolík, O., Pickett, J. S., Gurnett, D. A., Maksimovic, M., & Cornilleau-Wehrli, N. (2002). Spatiotemporal variability and propagation of equatorial noise observed by Cluster. *Journal of Geophysical Research*, 107(A12), 1495. <https://doi.org/10.1029/2001JA009159>
- Santolík, O., Pickett, J. S., Gurnett, D. A., Menietti, J. D., Tsurutani, B. T., & Verkhoglyadova, O. (2010). Survey of Poynting flux of whistler mode chorus in the outer zone. *Journal of Geophysical Research*, 115, A00F13. <https://doi.org/10.1029/2009JA014925>
- Sheeley, R. W., Moldwin, M. B., Rassoul, H. K., & Anderson, R. R. (2001). An empirical plasmasphere and trough density model: CRRES observations. *Journal of Geophysical Research*, 106, 25,631–25,642. <https://doi.org/10.1029/2000JA000286>
- Shprits, Y. Y. (2009). Potential waves for pitch-angle scattering of near-equatorially mirroring energetic electrons due to the violation of the second adiabatic invariant. *Geophysical Research Letters*, 36, L12106. <https://doi.org/10.1029/2009GL038322>
- Shprits, Y. Y., Runov, A., & Ni, B. (2013). Gyro-resonant scattering of radiation belt electrons during the solar minimum by fast magnetosonic waves. *Journal of Geophysical Research: Space Physics*, 118, 648–652. <https://doi.org/10.1002/jgra.50108>
- Shprits, Y. Y., Subbotin, D., & Ni, B. (2009). Evolution of electron fluxes in the outer radiation belt computed with the VERB code. *Journal of Geophysical Research*, 114, A11209. <https://doi.org/10.1029/2008JA013784>
- Spence, H. E., Reeves, G. D., Baker, D. N., Blake, J. B., Bolton, M., Bourdarie, S., ... Thorne, R. M. (2013). Science goals and overview of the Energetic Particle, Composition, and Thermal Plasma (ECT) suite on NASA's Radiation Belt Storm Probes (RBSP) mission. *Space Science Reviews*, 179, 311–336. <https://doi.org/10.1007/s11214-013-0007-5>
- Su, Z., Xiao, F., Zheng, H., & Wang, S. (2010a). Combined radial diffusion and adiabatic transport of radiation belt electrons with arbitrary pitch-angles. *Journal of Geophysical Research*, 115, A10249. <https://doi.org/10.1029/2010JA015903>
- Su, Z., Xiao, F., Zheng, H., & Wang, S. (2010b). STEERB: A three-dimensional code for storm-time evolution of electron radiation belt. *Journal of Geophysical Research*, 115, A09208. <https://doi.org/10.1029/2009JA015210>
- Su, Z., Xiao, F., Zheng, H., & Wang, S. (2011). Radiation belt electron dynamics driven by adiabatic transport, radial diffusion, and wave-particle interactions. *Journal of Geophysical Research*, 116, A04205. <https://doi.org/10.1029/2010JA016228>
- Su, Z., Xiao, F., Zheng, H., He, Z., Zhu, H., Zhang, M., ... Baker, D. N. (2014). Nonstorm time dynamics of electron radiation belts observed by the Van Allen Probes. *Geophysical Research Letters*, 41, 229–235. <https://doi.org/10.1002/2013GL058912>
- Su, Z., Wang, G., Liu, N., Zheng, H., Wang, Y., & Wang, S. (2017). Direct observation of generation and propagation of magnetosonic waves following substorm injection. *Geophysical Research Letters*, 44, 7587–7597. <https://doi.org/10.1002/2017GL074362>
- Su, Z., Zhu, H., Xiao, F., Zong, Q.-G., Zhou, X.-Z., Zheng, H., ... Wygant, J. R. (2015). Ultra-low-frequency wave-driven diffusion of radiation belt relativistic electrons. *Nature Communications*, 6, 10096. <https://doi.org/10.1038/ncomms10096>
- Su, Z., Zhu, H., Xiao, F., Zheng, H., Wang, Y., Shen, C., ... Wygant, J. R. (2015). Disappearance of plasmaspheric hiss following interplanetary shock. *Geophysical Research Letters*, 42, 3129–3140. <https://doi.org/10.1002/2015GL063906>
- Subbotin, D., Shprits, Y., & Ni, B. (2010). Three-dimensional VERB radiation belt simulations including mixed diffusion. *Journal of Geophysical Research*, 115, A03205. <https://doi.org/10.1029/2009JA015070>
- Thorne, R. M. (2010). Radiation belt dynamics: The importance of wave-particle interactions. *Geophysical Research Letters*, 37, L22107. <https://doi.org/10.1029/2010GL044990>
- Thorne, R. M., Li, W., Ni, B., Ma, Q., Bortnik, J., Chen, L., ... Kanekal, S. G. (2013). Rapid local acceleration of relativistic radiation-belt electrons by magnetospheric chorus. *Nature*, 504, 411–414. <https://doi.org/10.1038/nature12889>
- Tsurutani, B. T., Falkowski, B. J., Pickett, J. S., Verkhoglyadova, O. P., Santolík, O., & Lakhina, G. S. (2014). Extremely intense ELF magnetosonic waves: A survey of polar observations. *Journal of Geophysical Research: Space Physics*, 119, 964–977. <https://doi.org/10.1002/2013JA019284>
- Tsyganenko, N. A., & Sitnov, M. I. (2005). Modeling the dynamics of the inner magnetosphere during strong geomagnetic storms. *Journal of Geophysical Research*, 110, A03208. <https://doi.org/10.1029/2004JA010798>
- Tu, W., Cunningham, G. S., Chen, Y., Henderson, M. G., Camporeale, E., & Reeves, G. D. (2013). Modeling radiation belt electron dynamics during GEM challenge intervals with the DREAM3D diffusion model. *Journal of Geophysical Research: Space Physics*, 118, 6197–6211. <https://doi.org/10.1002/jgra.50560>
- Usanova, M. E., Mann, I. R., Rae, I. J., Kale, Z. C., Angelopoulos, V., Bonnell, J. W., ... Singer, H. J. (2008). Multipoint observations of magnetospheric compression-related EMIC Pc1 waves by THEMIS and CARISMA. *Geophysical Research Letters*, 35, L17S25. <https://doi.org/10.1029/2008GL034458>
- Varotsou, A., Boscher, D., Bourdarie, S., Horne, R. B., Glauer, S. A., & Meredith, N. P. (2005). Simulation of the outer radiation belt electrons near geosynchronous orbit including both radial diffusion and resonant interaction with whistler-mode chorus waves. *Geophysical Research Letters*, 32, L19106. <https://doi.org/10.1029/2005GL023282>
- Varotsou, A., Boscher, D., Bourdarie, S., Horne, R. B., Meredith, N. P., Glauer, S. A., & Friedel, R. H. (2008). Three-dimensional test simulations of the outer radiation belt electron dynamics including electron-chorus resonant interactions. *Journal of Geophysical Research*, 113, A12212. <https://doi.org/10.1029/2007JA012862>
- Wrenn, G. L. (1995). Conclusive evidence for internal dielectric charging anomalies on geosynchronous communications spacecraft. *Journal of Spacecraft and Rockets*, 32, 514–520. <https://doi.org/10.2514/3.26645>

- Wygant, J., Bonnell, J., Goetz, K., Ergun, R., Mozer, F., Bale, S., ... Tao, J. (2013). The electric field and waves instruments on the Radiation Belt Storm Probes mission. *Space Science Reviews*, 179(1-4), 183–220. <https://doi.org/10.1007/s11214-013-0013-7>
- Xiao, F., Yang, C., Su, Z., Zhou, Q., He, Z., He, Y., ... Blake, J. (2015). Wave-driven butterfly distribution of Van Allen belt relativistic electrons. *Nature Communications*, 6(8590). <https://doi.org/10.1038/ncomms9590>
- Yang, C., Su, Z., Xiao, F., Zheng, H., Wang, Y., Wang, S., ... Funsten, H. (2017). A positive correlation between energetic electron butterfly distributions and magnetosonic waves in the radiation belt slot region. *Geophysical Research Letters*, 44, 3980–3990. <https://doi.org/10.1002/2017GL073116>
- Yuan, Z., Yu, X., Huang, S., Wang, D., & Funsten, H. O. (2017). In situ observations of magnetosonic waves modulated by background plasma density. *Geophysical Research Letters*, 44, 7628–7633. <https://doi.org/10.1002/2017GL074681>
- Yue, C., Chen, L., Bortnik, J., Ma, Q., Thorne, R. M., Angelopoulos, V., ... Spence, H. E. (2017). The characteristic response of whistler mode waves to interplanetary shocks. *Journal of Geophysical Research: Space Physics*, 122, 10,047–10,057. <https://doi.org/10.1002/2017JA024574>
- Zhang, X. Y., Zong, Q.-G., Wang, Y. F., Zhang, H., Xie, L., Fu, S. Y., ... Pu, Z. Y. (2010). ULF waves excited by negative/positive solar wind dynamic pressure impulses at geosynchronous orbit. *Journal of Geophysical Research*, 115, A10221. <https://doi.org/10.1029/2009JA015016>